The Rings of Jupiter as Seen by the Electron and Proton Radiation Belt Model Salammbô

Quentin Nenon, Angélica Sicard, Pablo Caron

The rings of Jupiter as seen by the Electron and Proton Radiation Belt model Salammbô

Q. Nénon[1], A. Sicard[1] and P. Caron[1]

[1] ONERA, The French Aerospace lab, Toulouse, France

Corresponding author: Quentin Nénon (quentin.nenon@onera.fr)

Key points:

- The magnetic field model proposed by the Juno mission succesfully explains the final proton flux depletion observed by Galileo Probe
- Micrometer grains that populate the four rings do not shape the distribution of MeV particles observed by Pioneer 11 and Galileo Probe
- Most of the big grains of the main ring have a radius smaller than two centimeters

Abstract

A modeling of the effect of the rings of Jupiter on trapped >3 MeV electrons and protons is proposed. The effect is then added to the physical model Salammbô and discussed against in-situ measurements obtained by the Pioneer 11 and Galileo Probe missions. It is first shown that there is no evidence of an effect of the rings on the Jovian radiation belts, thanks to the new internal magnetic field model proposed by the Juno mission. Two grain populations are then studied: « small » grains, with a radius lower than 100 μm, are shown to not affect observable >3 MeV trapped particles. The normal optical depth of grains with a radius larger than two centimeters, that may exist in the main ring, is constained to be lower than 10^{-7} by the Salammbô model.

Plain language summary

Four very faint dust rings exist very close to the giant planet Jupiter. In the ring's region, very energetic electrons and protons are trapped by the planetary magnetic field in what are called "radiation belts". The first question addressed by this article is to determine if the rings affect the radiation belts of Jupiter. To do so, a numerical model of the radiation belts, named Salammbô, is used in conjunction with particle measurements gathered in-situ by Pioneer 11 in 1974 and Galileo Probe in 1995. This article shows that the micrometer grains that populate the rings do not affect available measurements. The second topic covered by this article is about how the Salammbô model constraints the distribution of centimeter grains in the brightest ring of Jupiter, named the main ring.

1 Introduction: the rings and radiation belts of Jupiter

The rings of Jupiter are generally separated in four different rings. The brightest one is the main ring that extends in the equatorial plan from around 1.72 to 1.82 Rj (1 Rj = 71492 km) away from the center of Jupiter [Esposito, 2014]. It has a total thickness of around 200 km [Brooks et al., 2004], maybe 800 km [de Pater et al., 2008]. The Halo ring extends inward of the main ring from around 1.25 to 1.72 Rj and has a large total thickness of around 20000 km or 0.28 Rj [Esposito, 2014]. The two previous rings are populated by grains created by micrometeoroid impacts on the small moons Metis and Adrastea that orbit at 1.8 Rj from the center of Jupiter. Finally, two very faint rings associated to impacts on the moons Amalthea

(orbiting at 2.54 Rj) and Thebe (orbiting at 3.11 Rj) exist and are named « Gossamer rings » or « secondary rings » [Showalter et al., 1985 Burns et al., 1999, Showalter et al., 2008]. They extend outward of the main ring and inward of their source moon from respectively 1.72 to 2.54 Rj (Amalthea ring) and 1.72 to 3.11 Rj (Thebe ring). Their thicknesses are driven by the orbital inclination of the moons orbits [Burns et al., 1999] and are of respectively around 5200 km for the Amalthea ring and 8800 km for the Thebe ring. Figure 1, panel a, shows the extension of the rings that we use in this study. We will point out hereafter that the assumed thickness of the main ring is not a critical assumption for this study.

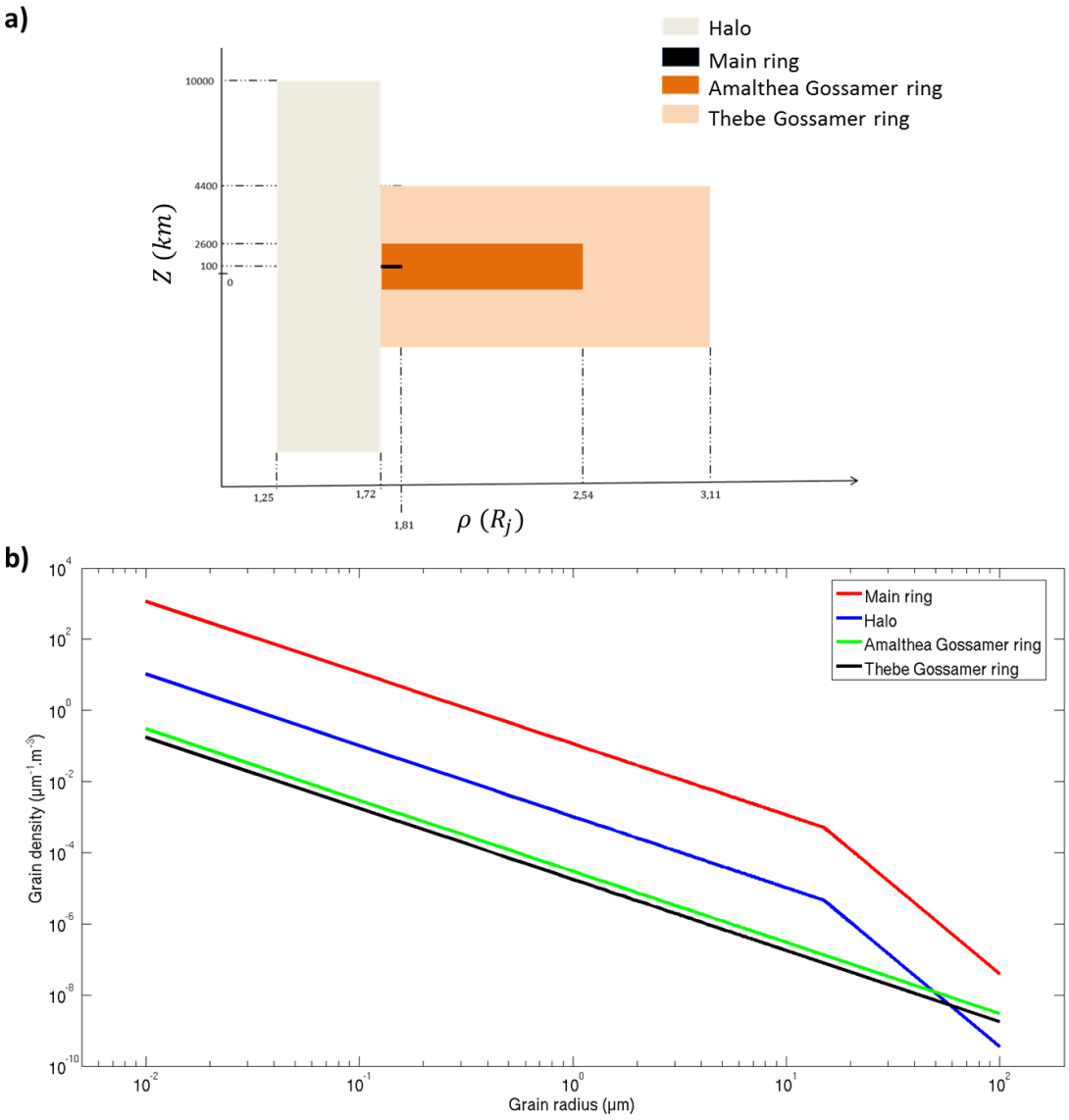

Figure 1 Panel a) Extension of the rings assumed in this study. The Z axis is along the spin axis of Jupiter and the rings are assumed to be axi-symmetric. Panel b) Assumed grain densities in the four rings of Jupiter.

Optical, infrared and near-infrared observations of the rings with various phase angles (angle between the Sun, the ring plan and the observer) have enabled the ring's community to study the size and densities of the grains. To do so, the grains are generally assumed to have a spherical shape, even if it is not true at least for the Gossamer rings [Showalter et al., 2008].

This assumption does not impact our study but enables us to sort the grains by their radius. The grains of the Gossamer rings have a typical radius of around 1 μm [de Pater et al., 2017], while the differential cross section of the grains in the main ring is maximum at a radius of 15 μm [Brooks et al., 2004]. The density of the grains is described by the function $n(r)$ where $n(r).dr$ gives the number of grains per volume having a radius between r and $r + dr$. $n(r)$ is therefore given in $\mu m^{-1}.m^{-3}$. Figure 1 b) shows the densities in the four rings for grain radius between 0.01 and 100 μm that we use in this article. The densities in the main ring are given by Brooks et al. [2004] and the densities in the Halo are scaled from that of the main ring, assuming that the grains that are drifting inward from the main ring are conserved but distributed along the large thickness of the Halo [Throop et al., 2004]. The densities in the Gossamer rings are from Showalter et al. [2008].

Grains larger than 100 μm (named hereafter "big" grains) have been detected in the main ring and have a normal optical depth at visible wavelengths of around $1.3\ 10^{-6}$ [Throop et al., 2004]. However, their density is unknown [Throop et al., 2004]. In addition, it is possible that the big grain densities do not follow a continuous power law, as tiny moons might exist in the rings (also called mooms or moonlets) [Burns et al., 1980 ; Showalter et al., 2007], and the grains can be clustered in clumps, detected by the New Horizons/LORRI experiment [Showalter et al., 2007].

de Pater et al. [2008] is the first and only existing effort to constrain the big grains of the main ring from measurements of the Jovian radiation belts. Resolved observations of the synchrotron radiation emitted by the trapped electrons and a preliminary computation led the previous authors to propose that a normal optical depth of $\tau_{cm} = 1.1\ 10^{-6}$ might come from grains with a radius larger than around two centimeters. If one compares the previous normal optical depth to the one reported by Throop et al. [2004] ($1.3\ 10^{-6}$), it means that more than 84% of the optical depth of big grains would come from centimeter and bigger grains.

In order to discuss the effect of the rings on the Jovian radiation belts and to infer properties of the big grains of the main ring, we first introduce the in-situ measurements of the radiation belts that can be used inward of the region of the main ring. Key hypotheses associated to the Salammbô electron and proton radiation belt models are then reminded in section 3 together with the modeling of the effects of the Jovian rings, that were not taken into account so far in the Salammbô model [Nénon et al., 2017 ; 2018]. Comparisons between the Salammbô model and the in-situ measurements are discussed in the last section, where the normal optical depth of the main ring centimeter grains is constrained.

2 In-situ measurements inward of the main ring

The in-situ measurements close to the main ring region and inward of it (L < 1.8, where L is the Mc Ilwain parameter) are very limited around Jupiter. There are observations obtained during the Pioneer 11 fly-by in 1974, measurements gathered by the atmospheric probe released by the Galileo mission in December 1995 (named hereafter « Galileo Probe ») and recent observations by the Juno mission.

The last version of the radiation belt model Salammbô has been developed by Nénon et al. [2017] for the trapped electrons and Nénon et al. [2018] for the trapped protons. We focus here only on electron and proton measurements, as there is so far no existing physical model for other species. The two previous species react differently to dust and we will analyze and

model relevant observations simultaneously and look for consistent solutions for both species. Inward of L=1.8, the Salammbô model computational grid is constructed so that only electrons with kinetic energies higher than 1.5 MeV and protons with energies above 4 MeV can be studied using the existing model (see Figure 1 of Nénon et al. [2018]). We therefore focus here only on observations of particles having a kinetic energy greater than the previous thresholds.

It leaves us with 4 electron channels and no proton channel onboard Pioneer 11 [Nénon et al., 2018]. The Trapped Radiation Detector (TRD) experiment was able to observe >8 and >35 MeV electrons [Fillius et al., 1975], while the Geiger Tube Telescope experiment (GTT) was able to observe >21 and >31 MeV electrons [Van Allen et al., 1975]. The GTT >31 MeV electron fluxes are in very good agreement with the TRD >35 MeV electron flux measurements, so that we only use the GTT >31 MeV observations in this study. In addition, the conclusions regarding the effect of the rings of Jupiter on the >21 MeV and >31 MeV measurements are very similar, so that only the >21 MeV fluxes are shown here.

The Energetic Particle Investigation (EPI) [Fischer et al., 1992] onboard Galileo Probe has six measurement channels of interest for this study, named E1, E2, E3, P1, P2 and P3. However, the channels do not separate well the different species [Fischer et al., 1996] and the geometric factors are not simple gate functions [Pehlke, 2000 ; Nénon et al., 2018]. Nénon et al. [2018] discuss the « P » channels responses and contaminations. In particular, is has been shown that P1 did not observe protons but electrons. In this study, we also use the « E » channels using the technique detailed in the Appendix A of Nénon et al. [2018], based on the geometric factors computed by Pehlke [2000]. The E2 and E3 channels have observed the same electron energy range, so only E3 is shown here. Similarly, P2 and P3 have observed the same proton energy range, so only P2 is shown. We use in this study the omnidirectional count rates provided by Pehlke [2000].

The kinetic energies observed by the « Jovian Energetic Particle Detector Instrument » (JEDI) [Mauk et al., 2013] onboard Juno are too low to be used in this study. The « Radiation Monitoring » experiment [Becker et al., 2017a] has observed >10 MeV electrons [Becker et al., 2017b]. However, the currently published and available measurements are below the detection limit of the experiment in the ring region [Becker et al., 2017b] because the particle loss cone covers almost all the equatorial pitch angles. We therefore do not use any Juno observation in this article.

3 The Salammbô model and the effect of the rings

3.1 The Salammbô model: is there any evidence in the in-situ measurements that rings affect energetic particle distributions?

The distribution of trapped particles in the radiation belts is governed by the balance of various physical processes, that can be represented by the Fokker-Planck equation detailed in Nénon et al. [2017]. For the Salammbô physical model, we use the internal magnetic field model O6 [Connerney, 1993]. The outer boundary condition of the Salammbô model is imposed at L=9.5 and is detailed in Nénon et al. [2017] for the electrons and Nénon et al. [2018] for the protons. The effects of the physical processes acting on the trapped particles are modeled by the loss and diffusion coefficients of the Fokker-Planck equation.

In the rings region, the following processes have already been included to the model [Nénon et al., 2017 ; 2018]: Coulomb collisions with the atmosphere of Jupiter and the magnetospheric cold plasma (electrons and protons), charge exchange and nuclear interactions with the atmosphere (protons), effects of the synchrotron radiation (electrons), charge exchange with the neutral gas torus of Io (protons), absorption by the moons (electrons and protons) and finally the radial diffusion process. The radial diffusion coefficient is taken here to be $D_{LL} = 1.3\ 10^{-10}\ L^4\ s^{-1}$, identical for the electrons and protons [Nénon et al., 2018]. It is a critical assumption that is further discussed in section 4.

The Cosmic Ray Albedo Neutron Decay (CRAND) source of protons is neglected in the Salammbô model and there is, so far, no need to add it to the model, meaning there is no observational evidence of this source close to Jupiter [Nénon et al., 2018]. The other only effect not taken into account in the Salammbô model is the effect of the rings, that is the purpose of this article.

Figure 2 shows the in-situ measurements in black compared to the fluxes simulated by the Salammbô model in red if we do not take into account any effect of the rings. We also superimpose in green the count rates that are due to heavy ions. One can see that the channels P1 and P2 are likely to be contaminated by these ions between 1.8 Rj and 2.3 Rj. Anywhere where the electron measurements are clean, including the Pioneer 11 measurements, one can see that there is no evidence of a strong missing effect of the rings (panels A to E). The electron flux is correctly simulated to decrease very close to the planet along the Galileo Probe trajectory because of kinetic energy losses and pitch angle frictions induced by the synchrotron radiation. However, this process is not effective on the trapped protons and a large discrepancy between the Salammbô-proton model and the Galileo Probe observations (panel F) inward of 1.6 Rj is observed. It might be an evidence for a missing strong effect of the rings on the energetic protons [Nénon et al., 2018]. In particular, the proton flux decrease observed by Galileo Probe when the spacecraft was 1.3 Rj away from the center of Jupiter is not reproduced at all (panel F). According to the internal magnetic field model O6 [Connerney, 1993] that is used for the Salammbô model, the observed trapped protons impact the atmosphere of Jupiter (meaning their guiding centers bounce or drift inward of 1.0 Rj) only when Galileo Probe was inward of 1.008 Rj.

However, the Juno mission has recently shown that the Jovian internal magnetic field topology significantly deviates from what was proposed by previous internal field models very close to the planet [Connerney et al., 2017 ; 2018]. Figure 2, panel G, shows the magnetic field line that passes by Galileo Probe when the spacecraft was at a distance of 1.077 Rj computed with three models: O6, that we use in Salammbô, VIP4 [Connerney et al., 1998], that has been adopted by the Juno teams in the pre-Juno period and the new magnetic field model proposed by the Juno mission, named JRM09 [Connerney et al., 2018]. All particles seen by Galileo Probe are allowed to bounce where the magnetic field amplitude is lower than the amplitude at the Probe position. It is below the horizontal dashed line on Figure 2, panel G. One can see that the particles bouncing at the Probe position would remain outside of the atmosphere of Jupiter according to the O6 and VIP4 model, while all particles observed by the Probe would impact the giant planet according to JRM09.

The bounce and drift trajectories of the guiding centers of the trapped particles bouncing at the position of Galileo Probe have then been followed. According to VIP4, the flux observed

by Galileo Probe should be 0 inward of 1.1 Rj. According to JRM09, the flux is 0 inward of 1.24 Rj, shown by the brown area on Figure 2 panel F labeled “JRM09”. It is an impressive result of this new magnetic field model that successfully explains the proton measurements obtained very close to Jupiter by Galileo Probe in 1995. We therefore do not see anymore an evidence of an effect of the rings in the in-situ measurements and do not use our model inward of 1.3 Rj. The effect of the high term degrees of the JRM09 model gradually decreases as we get further away from Jupiter, so that we still consider that using the O6 model between 1.3 Rj and around 2.0 Rj is a good assumption, at least near the magnetic equator.

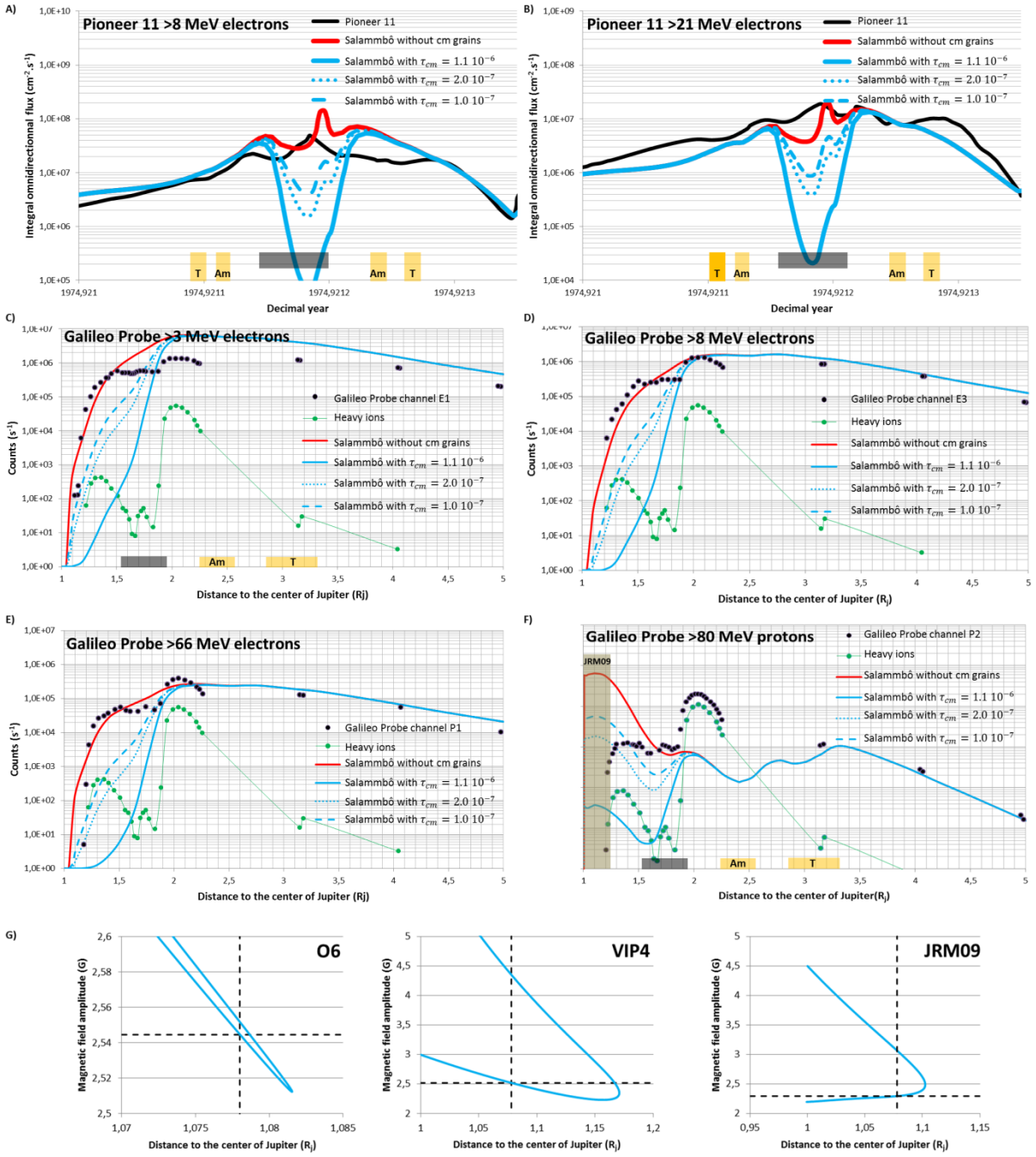

Figure 2 Panels A to F: Pioneer 11 and Galileo Probe in-situ measurements in black. The orange areas show when the spacecraft crosses magnetic field lines that might be intercepted by the moons Thebe (T) and Amalthea (Am). The grey area shows when field lines

intercepted by the small moons Metis and Adrastea are crossed, where is also the main ring. In the Galileo Probe plots, the green curve gives the estimate of the counts due to heavy ions, according to the technique detailed in Nénon et al. [2018]. The brown area with the label "JRM09" in the Galileo Probe plot shows where the spacecraft should have observed no trapped particles according to the internal magnetic field model JRM09. Superimposed in red is the Salammbô flux simulation if the effect of the rings is not taken into account. The blue curves show the simulations taking into account the absorption effect of centimeter grains, with three different assumed normal optical depths. The Salammbô simulations are done with the internal magnetic field model O6, and not the new model proposed by the Juno mission, named JRM09. Panel G: Magnetic field line passing by Galileo when the spacecraft was was at 1.077 Rj from the center of Jupiter according to three different internal magnetic field models. The crossing of the dashed lines shows the position of Galileo Probe.

3.2 Modeling the effect of the « small » grains of the rings

The very energetic electrons and protons easily go through the « small » grains (with a radius lower than $100\,\mu m$), as shown by the sketch of Figure 3 a, and experience during this interaction a loss of kinetic energy and a trajectory deviation (i.e. an equatorial pitch angle diffusion).

The kinetic energy loss is computed with the stopping power $\frac{dE}{dl}$ given by the NIST ESTAR database for the electrons and the NIST PSTAR database for the protons [Berger et al., 2000]. The grain sizes are small enough for energetic particles to have an almost constant kinetic energy during the grain crossing. The stopping power can therefore be assumed to be constant during the crossing of the grain. The grains are assumed to be made of silicate and to have a spherical shape. The trajectory deviation of the charged particles is sufficiently small to assume that the particle trajectory in matter is straight, as shown in the sketch of Figure 3 a). This assumption is verified in the Supporting Information 1 (Figure S1), as the deviation angles are smaller than around 10°. The average path within matter of a particle randomly impacting a grain with a radius r and having a straigth trajectory in it is of $\frac{4}{\pi}.r$. The last assumption of our modeling approach is that the rings of Jupiter are faint enough so that the probability to encounter two grains during a bounce motion is negligible compared to the probability to encounter only one. It is verified for the Jovian rings but is not true anymore for the dense rings of Saturn for instance. Using these assumptions, the Supporting Information 1 shows that the kinetic energy loss coefficient is given by (see equations S1 to S7):

$$\frac{dE}{dt} = \frac{\langle l \rangle}{\tau_b}\frac{dE}{dl}\int_{r_{min}=0.1\,\mu m}^{r_{max}=100\mu m} \frac{4}{\pi} * \pi * r^3\, n(r) dr \qquad [MeV.s^{-1}] \qquad (1)$$

Where $\langle l \rangle$ is the path length of the charged particle (with a given equatorial pitch angle on a given drift shell) within the ring during a bounce period. The $\langle \quad \rangle$ brackets mean that this length is averaged over the drift motion, to take into account the different configurations between the ring's plane and the magnetic equator plane. τ_b is the particle bounce period. Formula (1) shows that the kinetic energy loss rate is almost independent of the value chosen for r_{max} if the slope of the power law of $n(r)$ is higher in absolute value than 4. It is verified for the Halo and the main ring in which the slopes are of -5.0 for $r > 15\,\mu m$ (see Figure 1b) [Brooks et al., 2004]. Using a value of r_{max} of $100\,\mu m$ may lead to overestimate the

Gossamer rings effect, what does not impact the conclusions of this study. Finally, the main ring thickness is so small that the path length $\langle l \rangle$ is almost proportional to the assumed thickness H. As $n(r)$ is inversely proportional to H, the product $\langle l \rangle . n(r)$ and therefore $\frac{dE}{dt}$ are relatively independent of the assumed thickness of the main ring.

Supporting Information 1 (equations S8 to S13) details how, with a similar approach, we compute the pitch-angle diffusion coefficient D_{yy} associated to the effect of the "small" grains.

Figure 3, panel b, shows the computed kinetic energy loss $\left(\frac{1}{E}\frac{dE}{dt}\right)$ and pitch angle diffusion (D_{yy}) coefficients due to the effect of the « small » grains on 70° equatorial pitch angle particles. One can see that the equatorial pitch angle diffusion coefficients are small compared to the local radial diffusion for both the electrons and protons. We can therefore expect that the scattering of the trapped particles by the small grains of the rings do not significantly shape the energetic radiation belts of Jupiter. The kinetic energy loss terms for the electrons are small compared to the energy losses due to synchrotron radiation, so that the synchrotron radiation mechanism is the dominant one close to the planet. For the protons, one can see on Figure 3 b) that the kinetic energy loss is higher than the local radial diffusion in the Halo and main ring regions, so that it is possible that the small grains of these rings affect the innermost energetic proton radiation belts of Jupiter. However, in section 4 we will show that this effect is not seen in the Galileo Probe proton measurements, because the probe was very close to the magnetic equator and observed $\alpha_{eq} \approx 90°$ protons that do not cross the rings as often as the 70° protons.

3.3 Modeling the effect of centimeter grains in the main ring

Grains with a radius larger than around two centimeters absorb the impacting electron or proton, whatever is its energy (see Figure 3 a). If these grains are uniformly distributed around Jupiter, the probability for a particle to impact a grain can be expressed from the probability that has a photon going perpendicular to the ring plane to impact a grain (it is the definition of the normal optical depth, see equations S1 and S2). The absorption coefficient (probability to be absorbed per time unit) is this way given by (equation S3):

$$\frac{1}{\Gamma} = \frac{1}{\tau_b}\left[1 - exp\left(-\frac{\langle l \rangle}{H}\,\tau_{cm}\right)\right] \quad [s^{-1}] \qquad (3)$$

Where H is the total thickness of the ring and τ_{cm} is the normal optical depth of grains with a radius larger than 2 cm. The absorption coefficient is relatively independent of the assumed thickness of the main ring H, as the path length $\langle l \rangle$ is almost proportional to H in our simulations.

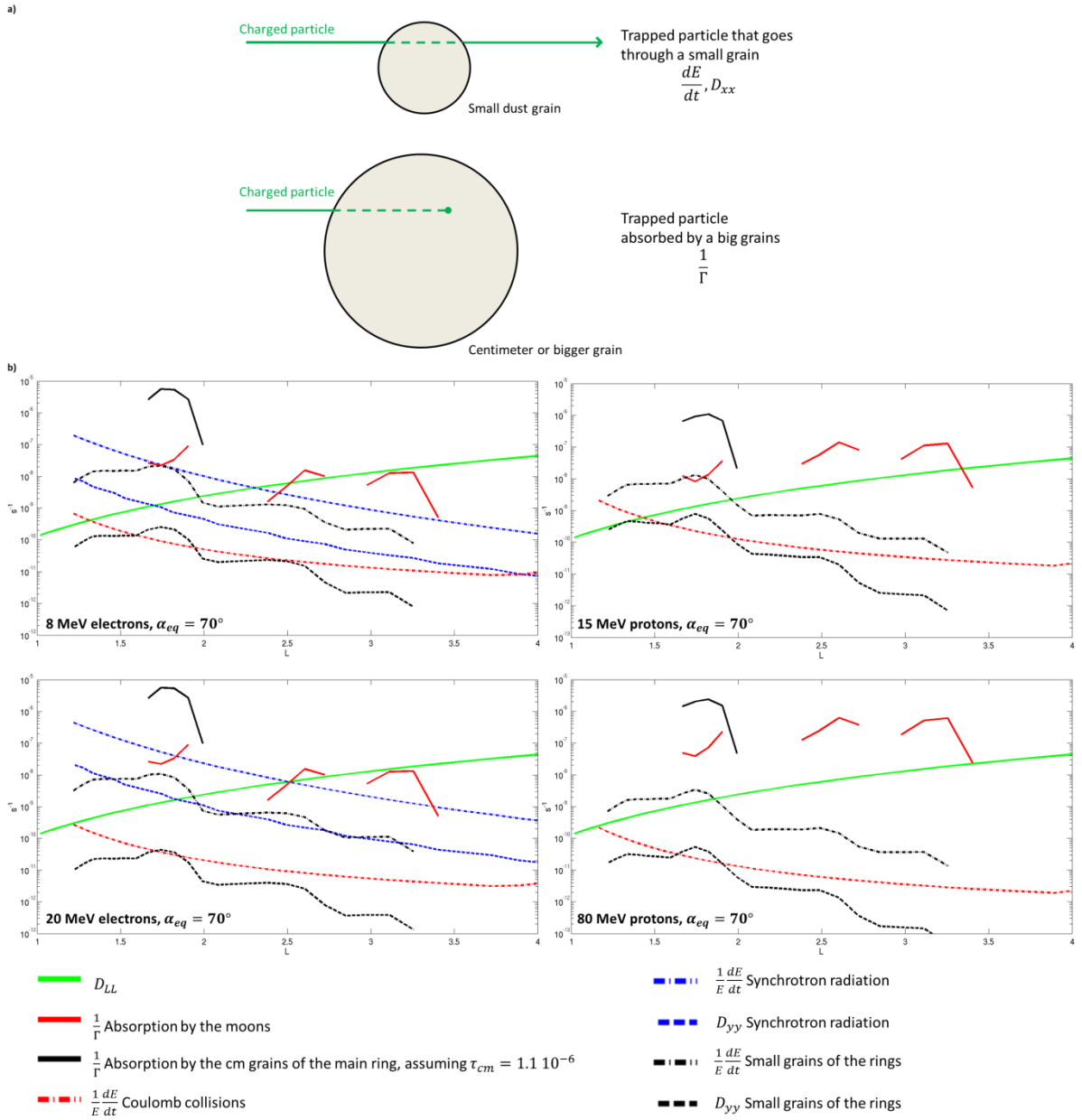

Figure 3 Panel a) A sketch showing that a charged particle impacting a "small" grain crosses it. During this interaction, the charged particle looses kinetic energy $\left(\text{energy loss rate } \frac{dE}{dt}\right)$ and its pitch angle is scattered (equatorial pitch angle diffusion coefficient D_{xx}). The sketch also shows the case of a charged particle impacting a centimeter grain. In this case, the particle is absorbed and lost from the radiation belts $\left(\frac{1}{\Gamma}\right)$. Panel b) Absorption, diffusion and loss coefficients associated to the physical processes acting on trapped electrons and protons in the innermost radiation belts of Jupiter. All the coefficients are normalized to be expressed in s^{-1}.

4 Discussion on the effect of the rings on the Jovian radiation belt in-situ measurements

The Salammbô Fokker-Planck equation has been solved taking into account or not the effect of the small grains. The flux simulations along the Pioneer 11 and Galileo Probe trajectories at the observed kinetic energies are identical in both cases. However, we remind here that the

small grains of the main ring and Halo may affect very energetic non-equatorial protons, that have not been observed so far. Finally, the coefficients shown in Figure 3 b) show that it is unlikely that the small grains shape the very energetic electron belts (typically >20 MeV), that can be remotely sampled by observations at high frequencies (around >1424 MHz) of the Jovian synchrotron radiation.

de Pater et al. [2008] proposes that $\tau_{cm} = 1.1\ 10^{-6}$, so that almost all of the optical depth of big grains of $1.3\ 10^{-6}$ [Throop et al., 2004] should come from $r > 2\ cm$ grains. Figure 2 shows in blue the effect of using $\tau_{cm} = 1.1\ 10^{-6}$ on the Salammbô simulations: large flux depletions are created close to Jupiter and are not consistent with the radiation belt in-situ measurements. Figure 2 also shows the simulation results using $\tau_{cm} = 2.0\ 10^{-7}$ (the dotted blue line) and $\tau_{cm} = 10^{-7}$ (dashed blue line). The main ring still adds observable particle losses for the last value, but the Salammbô simulation remains close to the in-situ measurements, so that it is an acceptable value. We therefore propose that, according to the Salammbô model, τ_{cm} should be lower than 10^{-7}. It means that less than 10% of the normal optical depth reported by Throop et al. [2004] should, according to Salammbô, come from grains uniformly distributed around Jupiter with radius larger than 2 cm.

The Salammbô model and the used radial diffusion rate therefore proposes that most of the big grains with a radius larger than around $100\ \mu m$ should be either:

- Smaller than two centimeters.
- Clustered in clumps or moonlets. It would be possible to model their effect as the absorption effect of Metis and Adrastea, but it would be negligible as the clumps are very small compared to the moons [Showalter et al., 2007].

The radial diffusion rate is a critical parameter to conclude on the negligible or dominant role of the rings. Existing other physical models of the electron radiation belts of Jupiter use an higher value for this parameter than this study [de Pater and Goertz., 1990;Santos-Costa and Bolton, 2008]. As the effect of the "small" grains tends to be negligible with the Salammbô radial diffusion rate, this conclusion would also be verified with an higher radial diffusion rate. Such a diffusion rate would allow for an higher normal optical depth for the centimeter grains than what we propose here with the Salammbô model.

Acknowledgments

Pioneer 11 >8 MeV and >21 MeV electron measurements are respectively from Fillius et al. [1975] and Nénon et al. [2017]. Galileo Probe count rates are scanned from Pehlke [2000].

Kinetic energy loss rates, pitch angle diffusion coefficients and absorption rates due to the effect of the rings and computed in this study are available at: https://doi.org/10.6084/m9.figshare.7097777.v1. One can also find at the previous link the scattering angles computed with Geant-4 and shown in Figure S1, and the Salammbô flux predictions along the trajectories of Pioneer 11 and Galileo Probe.

We thank S. M. Brooks, H. B. Throop and M. Showalter for discussions on the rings and P. Kollmann for discussions on the JRM09 magnetic field model.

We are thankful to D. Santos-Costa for discussions on the modeling of the effect of the rings.

References

Agostinelli, S. and collaborators (2003). Geant4 – a simulation toolkit, Nuclear Instruments and Methods in Physics Research Section A: Accelerators, Spectrometers, Detectors and Associated Equipment, 506 (3), 250-303, https://doi.org/10.1016/S0168-9002(03)01368-8

Becker, H. N., Alexander, J. W., Adriani, A., Mura, A., Cicchetti, A., Noschese, R., Jørgensen, J. L., Denver, T., Sushkova, J., Jørgensen, A., Benn, M., Connerney, J. E. P., Bolton, S. J., Allison, J.,Watts, S., Adumitroaie, V., Manor-Chapman, E. A., Daubar, I. J., Lee, C., Kang, S., McAlpine, W. J., Di Iorio, T., Pasqui, C., Barbis, A., Lawton, P., Spalsbury, L., Loftin, S., and Sun, J. (2017a). The Juno Radiation Monitoring (RM) Investigation, Space Science Reviews, 213(1-4), 507-545, https://doi.org/10.1007/s11214-017-0345-9

Becker, H. N., Santos-Costa, D., Jørgensen, J. L., Denver, T., Adriani, A., Mura, A., Connerney, J. E. P., Bolton, S. J., Levin, S. M., Thorne, R. M., Alexander, J. W., Adumitroaie, V., Manor-Chapman, E. A., Daubar, I. J., Lee, C., Benn, M., Sushkova, J., Cicchetti, A., and Noschese, R. (2017b). Observations of MeV electrons in Jupiter's innermost radiation belts and polar regions by the Juno radiation monitoring investigation : Perijoves 1 and 3. *Geophysical Research Letters*, 44(10), 4481-4488, https://doi.org/10.1002/2017GL073091

Berger, M. J., Coursey, J. S., & Zucker, M. A. (2000). ESTAR, PSTAR and ASTAR: Computer Programs for Calculating Stopping-Power and Range Tables for Electrons, Protons and α-Particles (Version 1.2. 2). National Institute of Standards and Technology, Gaithersburg

Beutier, T. (1993). Modélisation tridimensionelle pour l'étude de la dynamique des ceintures de radiation, ENSAE PhD manuscript

Brooks, S. M., Esposito, L. W., Showalter, M. R., and Throop, H. B. (2004). The size distribution of Jupiter's main ring from Galileo imaging and spectroscopy, *Icarus*, 170(1), 35-57, https://doi.org/10.1016/j.icarus.2004.03.003

Burns, J. A., Showalter, M. R., Hamilton, D. P., Nicholson, P. D., de Pater, I., Ockert-Bell, M. E., & Thomas, P. C. (1999). The formation of Jupiter's faint rings, Science, 284(5417), 1146-1150, https://doi/org/10.1126/science.284.5417.1146

Burns, J. A., Showalter, M. R., Cuzzi, J. N., & Pollack, J. B. (1980). Physical processes in Jupiter's ring: Clues to its origin by Jove!, Icarus, 44(2), 339-360, https://doi.org/10.1016/0019-1035(80)90029-9

Connerney, J. E. P., Kotsiaros, S., Oliversen, R. J., Espley, J. R., Joergensen, J. L., Joergensen, P. S., Merayo, J. M. G., Herceg, M., Bloxham, J., Moore, K. M., Bolton, S. J., and Levin, S. M. (2018). A New Model of Jupiter's Magnetic Field From Juno's First Nine Orbits. Geophysical Research Letters, 45(6), 2590–2596, https://doi.org/10.1002/2018GL077312

Connerney, J. E. P., Adriani, A., Allegrini, F., Bagenal, F., Bolton, S. J., Bonfond, B., Cowley, S. W. H., Gerard, J.-C., Gladstone, G. R., Grodent, D., Hospodarsky, G., Jorgensen, J. L., Kurth, W. S., Levin, S. M., Mauk, B., McComas, D. J., Mura, A., Paranicas, C., Smith, E. J., Thorne, R. M., Valek, P., and Waite, J. (2017). Jupiter's magnetosphere and aurorae

observed by the Juno spacecraft during its first polar orbits. Science, 356(6340), https://doi.org/10.1126/science.aam5928

Connerney, J. E. P., Acuna, M. H., Ness, N. F., and Satoh, T. (1998). New models of Jupiter's magnetic field constrained by the Io flux tube footprint, Journal of Geophysical Research : Space Physics, 103(A6), 11929-11939, https://doi.org/10.1029/97JA03726

Connerney, J. E. P. (1993). Magnetic fields of the outer planets, Journal of Geophysical Research : Planets, 98(E10), 18659-18679, https://doi.org/10.1029/93JE00980

de Pater, I., Hamilton, D. P., Showalter, M. R., Throop, H. B., and Burns, J. A. (2017). The Rings of Jupiter, Chapter 6 in : Planetary ring systems, Eds M. S. Tiscareno and C. D. Murray, Cambride University Press, Cambridge, UK, ISBN: 9781107113824

de Pater, I., Showalter, M. R., and Macintosh, B. (2008). Keck observations of the 2002–2003 jovian ring plane crossing. Icarus, 195(1), 348-360, https://doi.org/10.1016/j.icarus.2007.11.029

de Pater, Imke and Goertz, C. K (1990), Radial diffusion models of energetic electrons and Jupiter's synchrotron radiation: 1. Steady state solution. Journal of Geophysical Research: Space Physics, 95 (A1), pp. 39-50, https://doi.org/10.1029/JA095iA01p00039

Esposito, L. W. (2014). chapters 3 and 14 of Planetary rings, a post-equinox view, Editor L. W. Esposito, Cambridge University Press, Cambridge, UK, ISBN: 9781139236966

Fillius, R. W., Mogro-Campero, A., and Mc Ilwain, C. (1975). Radiation belts of Jupiter : a second look, *Science*, 188(4187), 465-467, https://doi.org/ 10.1126/science.188.4187.465

Fischer, H., Mihalov, J., Lanzerotti, L., Wibberenz, G., Rinnert, K., Gliem, F., & Bach, J. (1992). Energetic Particles Investigation (EPI). Space Science Reviews, 60(1–4), 79–90, https://doi.org/10.1007/bf00216850

Fischer, H. M., Pehlke, E., Wibberbez, G., Lanzerotti, L. J., & Mihalov, J. D. (1996). High-energy charged particles in the innermost Jovian magnetosphere. Science, 272(5263), 856–858, https://doi.org/10.1126/science.272.5263.856

Glauert, S. A., and Horne, R. B. (2005). Calculation of pitch angle and energy diffusion coefficients with the PADIE code, Journal of Geophysical Resesearch, 110(A4), https://doi.org/10.1029/2004JA010851

Highland, V. L. (1975). Some pratical remarks on multiple scattering, Nuclear Instruments and Methods, 129 (2), 497-499, https://doi.org/10.1016/0029-554X(75)90743-0

Mauk, B. H., Haggerty, D. K., Jaskulek, S. E., Schlemm, C. E., Brown, L. E., Cooper, S. A., et al. (2013). The Jupiter Energetic Particle Detector Instrument (JEDI) investigation for the Juno mission. Space Science Reviews, 213(1-4), 289–346, https://doi.org/10.1007/s11214-013-0025-3

Mott, N. F., & Massey, H. S. W. (1965). The theory of atomic collisions (Vol. 35), Oxford: Clarendon Press, https://doi.org/10.1090/S0002-9904-1934-05838-5

Nénon, Q., Sicard, A. and Bourdarie, S. (2017). A new physical model of the electron radiation belts of Jupiter inside Europa's orbit, Journal of Geophysical Research: Space Physics, 122, 5148-5167, https://doi.org/ 10.1002/2017JA023893

Nénon, Q., Sicard, A., Kollmann, P., Garrett, H. B., Sauer, S. P. A., and Paranicas, C. (2018). A physical model of the proton radiation belts of Jupiter inside Europa's orbit. Journal of Geophysical Research: Space Physics, 123. https://doi.org/10.1029/2018JA025216

Pehlke E. (2000). Teilchenpopulationen in der inneren Jupitermagnetosphäre. Untersuchung der EPI-daten von der Galileo Probe (PhD thesis).

Showalter, M. R., de Pater, I., Verbanac, G., Hamilton, D. P., and Burns, J. A. (2008). Properties and dynamics of Jupiter's gossamer rings from Galileo, Voyager, Hubble and Keck images, Icarus, 195(1), 361-377, https://doi.org/10.1016/j.icarus.2007.12.012

Showalter, M. R., Cheng, A. F., Weaver, H. A., Stern, S. A., Spencer, J. R., Throop, H. B., Birath, E. M., Rose, D., and Moore, J. M. (2007). Clump Detections and Limits on Moons in Jupiter's Ring System. *Science*, 318(5848), 232-234, https://doi.org/10.1126/science.1147647

Showalter, M. R., Burns, J. A., Cuzzi, J. N., & Pollack, J. B. (1985). Discovery of Jupiter's 'gossamer'ring. Nature, 316 , 526-528, https://doi.org/ 10.1038/316526a0

Throop, H. B., Porco, C. C., West, R. A., Burns, J. A., Showalter, M. R., and Nicholson, P. D. (2004). The jovian rings : new results derived from Cassini, Galileo, Voyager, and Earth-based observations, Icarus, 172(1), 59-77, https://doi.org/10.1016/j.icarus.2003.12.020

Van Allen, J. A., Randall, B. A., Baker, D. N., Goertz, C. K., Sentman, D. D., Thomsen, M. F., and Flindt, H. R. (1975). Pioneer 11 observations of energetic particles in the Jovian magnetosphere. *Science*, 188(4187), 459-462, https://doi.org/10.1126/science.188.4187.459

Text S1. Computing the kinetic energy loss and equatorial pitch angle diffusion coefficients associated to the small grains of the rings

The normal optical depth $\tau(\lambda)$ of a ring with a thickness H at an observation wavelength λ gives the normal extinction power of the ring by:

$$\frac{I_{out}}{I_{input}}(\lambda) = 1 - exp\big(-\tau(\lambda)\big)(S1)$$

Where I_{out} is the photon flux after the ring crossing and I_{input} the flux before the crossing. The ratio of I_{out} over I_{input} also gives the probability that has a photon to impact a grain during the crossing.

For the dust grains with a radius between 0.01 and $100\mu m$, the scattering theory of Mie can be used to determine the normal optical depth due to these grains from their densities $n(r)$ [Brooks et al., 2004]:

$$\tau(\lambda) = \int_{r_{min}=0.1\mu m}^{r_{max}=100\mu m} \pi r^2 * H * n(r) Q_{ext}(r,\lambda) dr \; (S2)$$

$Q_{ext}(r,\lambda)$ is given by the Mie theory and is the ratio of the scattering cross section of the grain to its geometric cross section πr^2.

In order to compute the probability that has a particle to impact a grain with a radius between r and $r + \Delta r$, one can adapt the previous definition of the normal optical depth by changing the integral boundaries, setting $Q_{ext} = 1$, and replacing the thickness H by the path length $l(\Delta t)$ that the trapped particle has inside the ring during the time interval Δt. The probability is this way given by:

$$P_{impact}(r, \Delta r, \Delta t) = 1 - exp\left[-\int_{r}^{r+\Delta r} \pi r^2 * l(\Delta t) * n(r) * dr\right] (S3)$$

If the radius interval is chosen small enough, the previous probability can be approximated by:

$$P_{impact}(r, \Delta r, \Delta t) \approx \pi r^2 l(\Delta t) * n(r) * \Delta r (S4)$$

If a particle impacts a grain with a radius between r and $r + \Delta r$ (with Δr relatively small), it looses during the grain crossing the amount ΔE of kinetic energy:

$$\Delta E(r) = \frac{\frac{4}{\pi} * r * dE}{dl} (E)[MeV] (S5)$$

The kinetic energy loss per time unit due to the population of grains with a radius between r and r+Δr is then given by:

$$\frac{dE}{dt}(r, \Delta r) = \frac{1}{\tau_b} * P_{impact}(r, \Delta r, \tau_b) * \Delta E(r)[MeV.s^{-1}] (S6)$$

$$\frac{dE}{dt}(r, \Delta r) = \frac{\frac{1}{\tau_b} * dE}{dl} * l \frac{(\tau_b) * 4}{\pi} \pi r^3 n(r) \Delta r [MeV.s^{-1}] (S7)$$

By summing over all the radius intervals Δr and using a sufficiently small value for the interval width, one gets the equation given in the article.

The trajectory deviation distribution is computed using the multiple collision theory [Mott and Massey, 1965 ; Highland, 1975] that predicts that the deviation angles distribution is a Normal distribution with a standard deviation θ_0 given by:

$$\theta_0 = E_s \frac{E + E_0}{E(E + 2E_0)} \sqrt{\frac{\frac{4}{\pi} r}{l_0}} (S8)$$

With E the particle kinetic energy, E_0 its rest energy, $E_s = 15MeV$, r the radius of the grain (so that $\frac{4}{\pi} r$ is the path length within the grain) and l_0 the radiation length of silicate, $l_0 = 27g.cm^{-2}$. One can see here that the scattering angle standard deviation depends on the particle type (electron or proton) through the rest mass E_0, that is around 0.51 MeV for an electron and 938 MeV for a proton.

Simulations have been conducted with the Geant-4 ("Geometry And Tracking") toolkit [Agostinelli et al., 2003] to check that the multiple collision theory can be used for very energetic electrons and protons impacting ring grains with a radius lower than $100\mu m$. Figure S1 shows the histogram of the Geant-4 simulations in blue for electrons of 8 MeV and protons of 15 MeV impacting a grain with a radius of $15\mu m$ and $100\mu m$. The Normal distribution predicted by the multiple collision theory is overplotted in red. One can see that the multiple collision theory standard deviation is in very good agreement with the Geant-4 simulations. We can therefore use this theory for our application.

The trajectory deviation angle has a differential probability to be between Ψ and $\Psi + d\Psi$ given by:

$$P_{scattering}(\Psi) = \frac{1}{\sqrt{2\pi}\theta_0(r)} exp\left(\frac{-\Psi^2}{2\theta_0(r)^2}\right) (S9)$$

A deviation of an angle Ψ at a position on the magnetic field line given by B_l, the local magnetic field amplitude, and B_e, the amplitude at the magnetic equator, creates a change in the cosine of the equatorial pitch angle x given by [Beutier, 1993]:

$$\left(\Delta x(\Psi)\right)^2 = \frac{1}{2x^2}\left(x^2 - 1 + \frac{B_e}{B_l}\right)\left[2\left(x^2 - 1 + \frac{B_e}{B_l}\right)(1 - cos\Psi)^2 + (1 - x^2)sin^2\Psi\right] (S10)$$

The equatorial pitch angle diffusion coefficient D_{xx} is given by [Glauert and Horne, 2005]:

$$D_{xx} = \frac{1}{2}\left\langle \frac{(\Delta x)^2}{\Delta t} \right\rangle [s^{-1}](S11)$$

The equatorial pitch angle diffusion created by grains with a radius between r and $r + \Delta r$ is obtained with:

$$D_{xx}(r, \Delta r) = \frac{1}{\tau_b}\frac{1}{2} n(r)\pi r^2 \int_{-\pi}^{\pi} P_{scattering}(\Psi, r)\left(\Delta x(\Psi)\right)^2 d\Psi \, \Delta r [s^{-1}](S12)$$

In the previous equation, the product $n(r).\pi.r^2$ is used to take into account the probability to impact a grain, as we did for the computation of the kinetic energy losses. By summing over all the Δr intervals, one finally gets the equatorial pitch angle diffusion coefficient:

$$D_{xx} = \frac{1}{2}\frac{\langle l \rangle}{\tau_b} \int_{r_{min}=0.1\mu m}^{r_{max}=100\mu m} n(r)\pi r^2 \int_{-\pi}^{\pi} \left(\Delta x(\Psi)\right)^2 P_{scattering}(\Psi, r)\, d\Psi dr \, [s^{-1}](S13)$$

One can convert D_{xx} to D_{yy}, where $y = sin(\alpha_{eq})$, by: $D_{yy} = \left(\frac{cos\alpha_{eq}}{sin\alpha_{eq}}\right)^2 D_{xx}$.

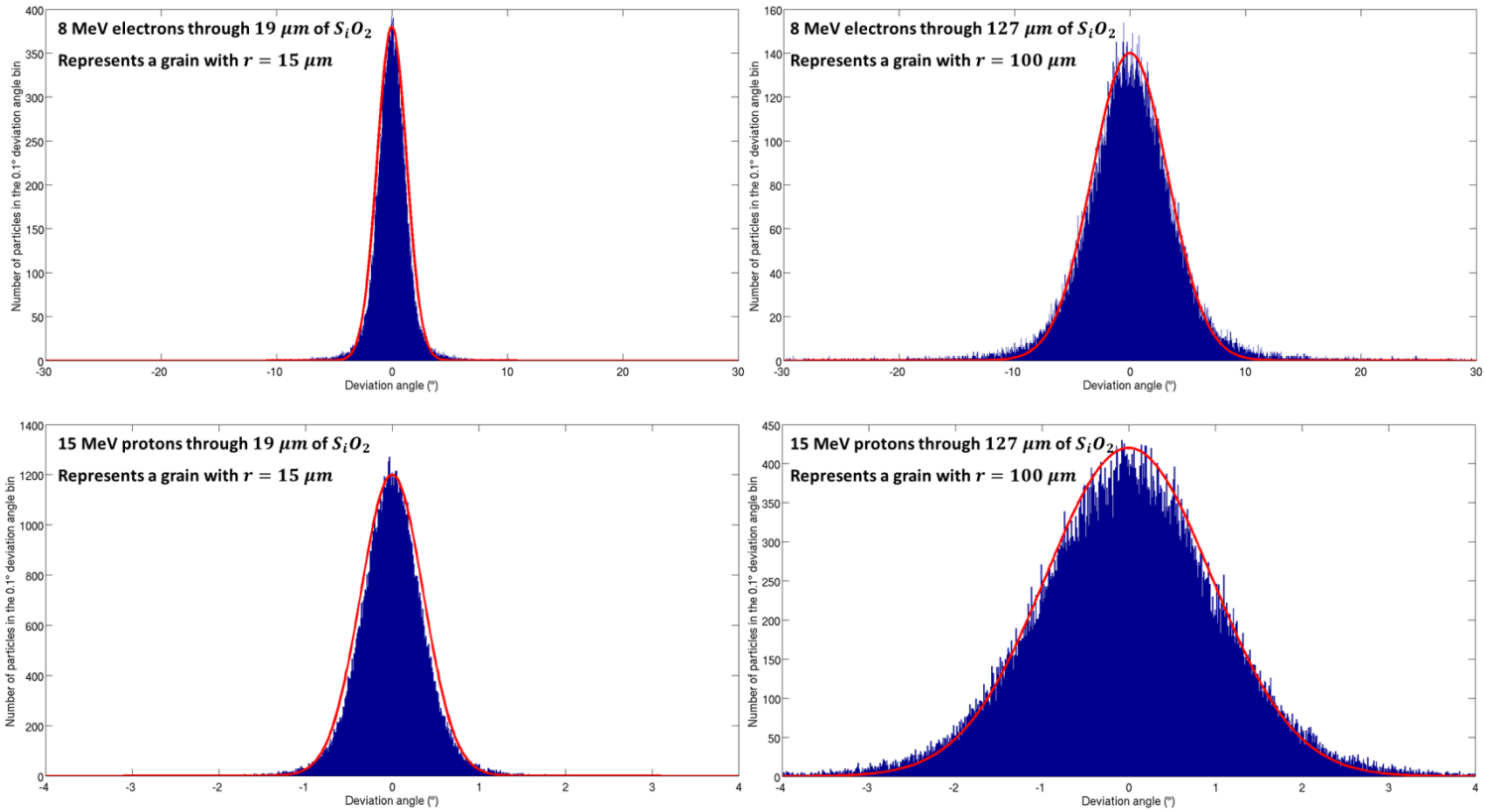

Figure S1. In blue, histogram of the deviation angles computed by the Geant-4 simulations and using 0.01° wide bins. In red, a Normal distribution with the standard deviation predicted by the multiple collision theory, scaled to the maximum of the histogram.

References

Agostinelli, S. and collaborators (2003). Geant4 – a simulation toolkit, Nuclear Instruments and Methods in Physics Research Section A: Accelerators, Spectrometers, Detectors and Associated Equipment, 506 (3), 250-303, https://doi.org/10.1016/S0168-9002(03)01368-8

Beutier, T. (1993). Modélisation tridimensionelle pour l'étude de la dynamique des ceintures de radiation, ENSAE PhD manuscript

Brooks, S. M., Esposito, L. W., Showalter, M. R., and Throop, H. B. (2004). The size distribution of Jupiter's main ring from Galileo imaging and spectroscopy, *Icarus*, 170(1), 35-57, https://doi.org/10.1016/j.icarus.2004.03.003

Highland, V. L. (1975). Some pratical remarks on multiple scattering, Nuclear Instruments and Methods, 129 (2), 497-499, https://doi.org/10.1016/0029-554X(75)90743-0

Glauert, S. A., and Horne, R. B. (2005). Calculation of pitch angle and energy diffusion coefficients with the PADIE code, Journal of Geophysical Resesearch, 110(A4), https://doi.org/10.1029/2004JA010851

Mott, N. F., & Massey, H. S. W. (1965). The theory of atomic collisions (Vol. 35), Oxford: Clarendon Press, https://doi.org/10.1090/S0002-9904-1934-05838-5